COMMUNICATION

Check for updates

Enhanced photochemical CO_2 reduction in the gas phase by graphdiyne†

Shaowen Cao, [iD] *[a] Yajie Wang,[a] Bicheng Zhu,[a] Guancai Xie,[bc] Jiaguo Yu [iD] *[a] and Jian Ru Gong [iD] *[bc]

Photocatalytic CO_2 reduction is promising for reducing the greenhouse effect and producing renewable energy, but still shows low activity and selectivity due to the ineffective utilization of photogenerated charge carriers and insufficient active sites for CO_2 adsorption and activation. Taking CdS nanocrystals as a model semiconductor, we demonstrate that graphdiyne, a new type of two-dimensional carbon allotrope uniquely formed from sp- and sp^2-hybridized carbon, enhances CO_2 photoreduction over CdS with higher activity, selectivity, and stability in the gas phase without any sacrificial agent compared to graphene. Both experimental and theoretical results prove that the chemical bonding between graphdiyne and CdS and sufficient CO_2 adsorption sites due to the strong interfacial interaction-induced sulfur vacancies in CdS and more electron-deficient acetylenic linkages in graphdiyne lead to more efficient electron transfer and storage for the subsequent CO_2 reduction reaction. The excellent properties of graphdiyne make it promising for applications in solar energy conversion.

Photochemical conversion of CO_2 into solar fuels is a clean, carbon-neutral, and sustainable strategy to mitigate the global energy and environmental issues simultaneously. In a general process, solar light is harvested by a semiconductor photoabsorber to produce photogenerated charge carriers, which subsequently trigger surface catalytic reactions to reduce CO_2 to CO and hydrocarbons by photoexcited electrons and to oxidize water to oxygen by photoexcited holes.[1–3] However, the construction of an efficient photochemical system for CO_2 reduction is still a challenge, because single-component

semiconductors are less effective in utilizing photoexcited charges and linear CO_2 molecules are chemically rather inert against activation during photocatalysis.[4–6] Hence, the employment of cocatalysts, for example, noble metals (Pt, Pd, Au, *etc.*), earth-abundant metals (Cu, Co, Ni, *etc.*), and enzymes, is necessary to accelerate the surface catalytic processes of CO_2 photoreduction.[7] Nevertheless, noble metals and enzymes are scarce and expensive, while non-noble metal-based cocatalysts are less active and stable, which limit their practical applications. A promising candidate is the family of cost-effective nanocarbons (carbon dots, carbon nanotubes, and graphene), which not only greatly promote the charge transfer, but also increase the active sites.[7] Especially, due to its excellent conductivity and electron mobility arising from its sp^2 hybridized two-dimensional (2D) carbon atom network, graphene can serve as an electron acceptor or transport channel to promote charge transfer and separation, thus improving photocatalytic efficiency, which is even comparable to those of high-performance noble metal cocatalysts.[8–11] The ability of graphene to accumulate photoelectrons is particularly attractive to increase the kinetics of the multi-electron transfer process of CO_2 photoreduction. In addition, improving CO_2 binding to a photocatalytic material is of vital importance to promote the catalytic efficiency in surface CO_2 conversion reactions.[12,13]

Graphdiyne (GDY), a stable synthetic 2D carbon allotrope,[14,15] shows interesting features similar to graphene such as a large surface area and high electron mobility, which make graphdiyne a good host matrix for semiconductor nanostructures, as well as an excellent electron acceptor or electron transfer medium,[16–19] promising for applications in the fields of electrocatalysis,[20–22] photocatalytic degradation,[23–28] water splitting,[29–31] and most recently CO_2 photoreduction.[32] More importantly, it should be noted that graphdiyne has a highly π-conjugated structure composed of sp- and sp^2-hybridized carbon atoms, while graphene only has a purely sp^2-hybridized carbon framework. This enables the presence of acetylenic linkages in graphdiyne, which are more electron-deficient than ethylenic linkages and do not exist in graphene, and therefore

[a] State Key Laboratory of Advanced Technology for Materials Synthesis and Processing, Wuhan University of Technology, 430070 Wuhan, P. R. China. E-mail: swcao@whut.edu.cn; jiaguoyu@yahoo.com

[b] CAS Center for Excellence in Nanoscience, CAS Key Laboratory of Nanosystem and Hierarchy Fabrication, National Center for Nanoscience and Technology, 100190 Beijing, P. R. China. E-mail: gongjr@nanoctr.cn

[c] University of Chinese Academy of Sciences, 100049 Beijing, P. R. China

† Electronic supplementary information (ESI) available. See DOI: 10.1039/d0ta02256j

This journal is © The Royal Society of Chemistry 2020

J. Mater. Chem. A, 2020, **8**, 7671–7676 | **7671**

graphdiyne can capture electrons more easily than graphene.[33,34] Moreover, the uniformly distributed pores among the three diacetylenic linkages ($-C\equiv C-C\equiv C-$) provide abundant hollow sites for CO_2 adsorption,[35] while graphene only possesses six-membered carbon rings with smaller void space (Fig. S1†). Also, the improved electronic properties resulting from the diacetylenic links induce higher CO_2 adsorption selectivity compared to graphene without such links.[36] These advantages in principle make graphdiyne promising to promote CO_2 photoreduction over semiconductor photoabsorbers.

As a proof of concept in this study, we demonstrate that graphdiyne performs better than graphene as a cocatalyst, to enhance CO_2 photoreduction over a model semiconductor photoabsorber, CdS nanocrystals, in the gas phase without any sacrificial agent. Higher activity, selectivity, and stability for CO_2 photoreduction can be achieved over graphdiyne-modified CdS (denoted as CdGDY), as compared to graphene-modified CdS (denoted as CdG). Such a performance enhancement is attributed to the chemical bonding between graphdiyne and CdS and sufficient CO_2 adsorption sites due to the strong interfacial interaction-induced sulfur vacancies in CdS and more electron-deficient acetylenic linkages in graphdiyne, which essentially improve the electron transfer and storage for the subsequent CO_2 reduction reaction.

CdGDY was synthesized by growing CdS nanocrystals *in situ* on the surface of graphdiyne, under DMSO-involved solvothermal conditions. Here DMSO was used as both a solvent and a reactant of the S source. The composition of the composite was elucidated from Raman spectra (Fig. S2†), together with graphene oxide (GO), graphdiyne, CdG, and CdS for comparison. Particularly, the Raman spectra of GO, graphdiyne, CdG, and CdGDY show a D peak at 1344 cm^{-1}, a signature of disorder, and a G peak at 1585 cm^{-1}, in-plane stretching vibrations of sp^2-hybridized carbon atoms, respectively. The result indicates the existence of lattice defects and an sp^2 carbon network in all the samples.[37,38] The characteristic peaks of acetylenic linkages in graphdiyne are located at 1917 and 2170 cm^{-1}. For CdS, CdG, and CdGDY, three Raman peaks located at 296, 592 and 900 cm^{-1} correspond to the longitudinal optical (LO) phonon modes of first-order (1LO), second-order (2LO) and third-order (3LO) of CdS,[39,40] revealing the existence of CdS. Transmission electron microscopy (TEM) images show the 2D-layered structure of graphdiyne (Fig. S3a†). This morphology serves to prevent the aggregation of CdS nanocrystals during the *in situ* formation process. As seen in Fig. S3b–f,† pure CdS shows significant aggregation to form spheres with a larger size, whereas fine CdS nanocrystals are seen homogenously distributed on the surfaces of both graphdiyne and graphene. The small size of CdS nanocrystals in the presence of graphdiyne or graphene was also confirmed from XRD data (Fig. S4†). The diffraction peaks of CdGDY and CdG are broader than that of pure CdS, which is attributed to the smaller crystallite size. In addition, both CdGDY and CdG show a much higher specific surface area and larger pore volume than pure CdS and the specific surface area of CdGDY is relatively larger than that of CdG, as determined from N$_2$ adsorption–desorption measurements at 77 K (Fig. S5 and Table S1†). It is

noted here that well-dispersed CdS nanoparticles can be observed on the graphdiyne surface even after 3 h continuous sonication, while some CdS nanoparticles detach from the surface of graphene under the same conditions, as shown in Fig. S6.† This observation shows stronger interaction between CdS and graphdiyne, indicating the good structural stability of CdGDY.

XPS analysis was performed to elucidate the chemical states and interfacial interaction in the samples. As shown in Fig. 1a, C 1s spectra of GDY and CdGDY are deconvoluted into four peaks, attributed to C=C (sp^2-hybridized carbon, 284.5 eV), C≡C (sp-hybridized carbon, 285.0 eV), C–O (epoxy or hydroxyl groups, 286.9 eV), and C=O (carboxyl or carbonyl groups, 288.8 eV).[23] For both GDY and CdGDY, the peak area of sp^2-hybridized carbon is twice that of sp-hybridized carbon, which is consistent with the structure of graphdiyne shown in the diagram in Fig. S1.† Three deconvoluted peaks of C 1s corresponding to GO (Fig. 1b) are centered at 284.8 eV (C=C), 286.8 eV (C–O), and 288.4 eV (C=O).[41] Note that the relative peak intensity ratios of oxygen-containing groups are much lower for CdGDY and CdG, as compared to those for GDY and GO, suggesting an increased degree of reduction in the composites, which is beneficial for improving electron mobility and conductivity. With regard to S 2p and Cd 3d spectra (Fig. 1c and d), pure CdS shows peaks of S^{2-} at 161.4 (2p$_{3/2}$) and 162.6 eV (2p$_{1/2}$),[42] and the Cd–S bond at 405.1 (Cd 3d$_{7/2}$) and 411.9 eV (Cd 3d$_{5/2}$).[43] It is noteworthy that both S 2p and Cd 3d spectra of CdG are shifted by 0.6 eV to higher binding energy, and the C–O peak shifts to lower energy by 0.5 eV, revealing the interfacial charge transfer from CdS to graphene. Importantly, new peaks (404.5 and 411.3 eV) originating from the Cd–O bond appear in CdGDY,[44] together with the Cd–S bond shifted to higher energy by 0.4 eV (due to interfacial charge transfer). Moreover, the peak of C=C in CdGDY shifts to lower energy by 0.4 eV. These results indicate chemical bonding (Cd–O–C) between CdS and graphdiyne
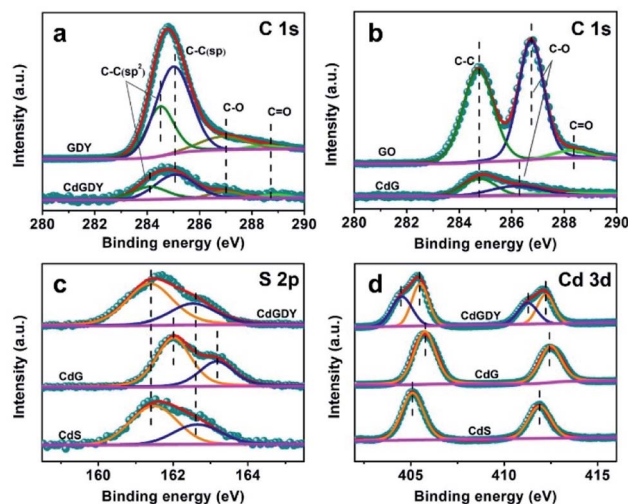

Fig. 1 High-resolution XPS C 1s spectra of graphdiyne and CdGDY (a) and GO and CdG (b); S 2p spectra (c) and Cd 3d spectra (d) of CdS, CdG and CdGDY.

7672 | *J. Mater. Chem. A*, 2020, **8**, 7671–7676

This journal is © The Royal Society of Chemistry 2020

accompanied by the interfacial charge transfer from CdS to graphdiyne, which explains the stronger interfacial interaction between graphdiyne and CdS compared to that between graphene and CdS. Note that the position of S 2p of CdGDY doesn't change obviously compared to that of CdS. This is because of the formation of the Cd–O bond, i.e., the introduction of O would balance the electron density change in CdS with S vacancies, thus leading to an unobvious change of the binding energy.

We further simulated the interfacial electronic interaction between CdS and the two carbonaceous materials through DFT calculations. As indicated by the aforementioned XPS analysis, the Cd–O–C bond formed between CdS and graphdiyne was not found at the CdS/graphene interface. Modelling on this premise (Fig. 2a and b), the calculated charge density differences in CdGDY are shown in yellow and cyan areas, representing electron accumulation and depletion, respectively. At the Cd/GDY interface, the CdS surface consists mainly of the cyan area and the graphdiyne surface is mainly filled by the yellow area. Moreover, the planar-averaged electron density difference at the Cd/GDY interface is also shown in Fig. 2c, where positive and negative values represent electron accumulation and depletion, respectively. The charge distribution at the interface indicates that electrons mainly transfer from CdS to graphdiyne through

the interface. According to the calculated results from Fig. 2d–f, the electron transfer direction in CdG is similar to that in CdGDY. However, the electron density at the interface of CdG is much smaller than that of CdGDY. Quantitative results from Bader charge analysis reveal that a charge of $\sim$2.40e is transferred from CdS to graphene through the CdS(111)/graphene interface, while a charge of $\sim$3.86e is transferred from CdS to graphdiyne through the CdS(111)/graphdiyne interface. Our computational modelling results indicate stronger electronic coupling and faster interfacial charge transfer between CdS and graphdiyne compared to those in CdG, which is consistent with the XPS analysis.

The interfacial interaction in CdS–graphdiyne was further demonstrated by electron paramagnetic resonance (EPR) measurements, as shown in Fig. 3a. The EPR signals at 3436 Gauss ($g = 2.003$) over GDY and graphene can be attributed to oxygen-containing defects. These signals nearly disappear in the curves of the hybrid materials due to the low loading amount of carbon materials and the reduction of oxygen-containing groups during the solvothermal process. The weak EPR signal at 3432 Gauss ($g = 2.005$) observed in CdS can be ascribed to sulfur vacancies.[45,46] The intensity of this signal remains nearly unchanged in the presence of graphene, but it is significantly enhanced in the presence of graphdiyne. This enhancement is due to the increase in sulfur vacancies, which are formed to counter the charge imbalance resulting from the formation of (Cd–O–C) chemical bonds at the interface. Sulfur vacancies can act as electron traps to promote the separation of photogenerated charge carriers[47,48] and also improve the adsorption of CO_2 molecules.[49,50]

Then, the free charge carrier density of the samples was investigated by testing the band structure based on UV-vis diffuse reflectance spectra and the Mott–Schottky (M–S) relationship. Fig. S7† suggests that the absorption edge of CdS (542 nm) undergoes a blue shift to 522 nm and 517 nm, in the
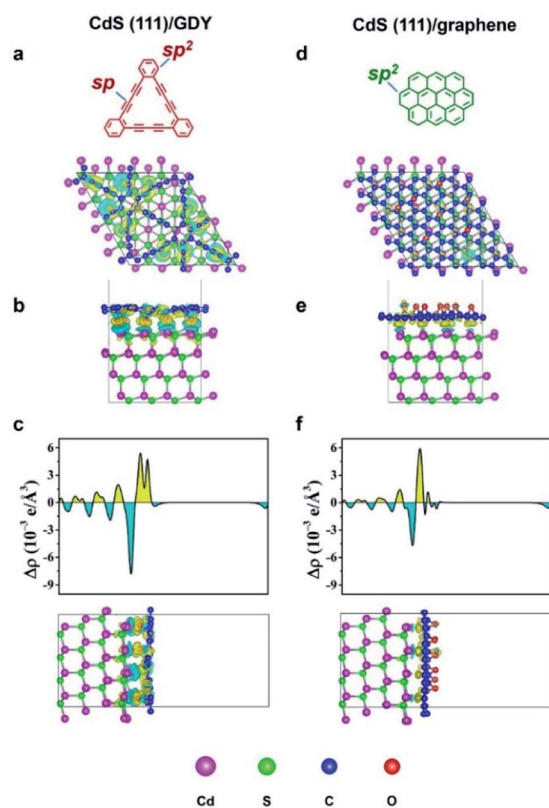

Fig. 2 Top view (a and d) and side view (b and e) of the charge density difference and planar-averaged electron density difference along with Z direction (c and f) for CdS(111)/graphdiyne and CdS(111)/graphene. The yellow and cyan regions represent electron accumulation and depletion, respectively. The isosurface value is 0.002 e Å^{-3}.
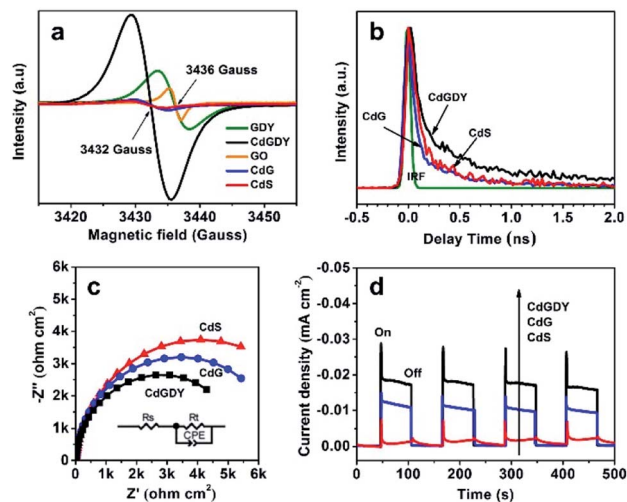

Fig. 3 (a) EPR spectra of CdS, CdG, CdGDY, GDY and GO; (b) TRPL spectra, (c) EIS and (d) transient photocurrent response curves of CdS, CdG, and CdGDY.

This journal is © The Royal Society of Chemistry 2020

J. Mater. Chem. A, 2020, 8, 7671–7676 | 7673

presence of graphdiyne and graphene, respectively. The direct-transition bandgaps (E_g) of CdS in pure CdS, CdGDY, and CdG are thus calculated to be 2.29, 2.37 and 2.40 eV, respectively. The absorption blue shift and bandgap increase are attributed to the quantum size effect of CdS nanocrystals in the composites, in agreement with the XRD results. The typical n-type semiconductor behavior of CdS was confirmed by the positive slope of the M–S curve shown in Fig. S8.†[51] Normally, in n-type semiconductors, the flat-band potential can be approximately regarded as the conduction band (CB) potential.[52,53] It can be seen that the flat-band potentials of CdS determined from the intercept on the X-axis of the tangent to the M–S curves are −1.1 V (*vs.* Ag/AgCl, pH = 7) for all the samples. Hence, the CB potential of CdS is calculated to be −0.49 V (*vs.* the reversible hydrogen electrode, RHE). It is known that the density of charge carriers is inversely proportional to the slope of the M–S curves (see experimental details in the ESI†). In the case of CdGDY, since the slope of the curve is much smaller than that for CdS and CdG, we conclude that a higher density of charge carriers is present in CdGDY, which is consistent with the afore-discussed DFT calculation results.

To elucidate the charge transfer properties of the as-prepared samples, time-resolved photoluminescence (TRPL) spectroscopic and photoelectrochemical measurements were conducted. The TRPL decay curves (Fig. 3b) are well fitted with bi-exponential decay kinetics (Table S2†). The short lifetime (τ_1) and long lifetime (τ_2) reflect the radiative and non-radiative processes, respectively. In comparison with CdS, CdG shows both shorter lifetimes, indicating the relaxation of the CdG excitations *via* non-radiative decay channels, presumably by rapid charge transfer from CdS to the surface of graphene. Moreover, the luminescence lifetimes of CdGDY are prolonged as compared to those of CdG and pure CdS, ascribed to the defect-induced electron trap states. These defects can capture photogenerated electrons to effectively split excitons and prevent their recombination,[47,48,54] resulting in a slower decay rate of luminescence and thus a longer lifetime. The average lifetime values (τ_m) are determined to be 0.50, 0.31, and 0.33 ns for CdGDY, CdG, and CdS, respectively. These results reveal that both the interfacial transfer and defect capture help to improve the charge separation and suppress the charge recombination, although in different manners. And the results from the corresponding steady-state PL spectra are consistent with those from the TRPL spectra (Fig. S9†). Furthermore, the smaller radius of electrochemical impedance spectroscopic (EIS) Nyquist plots and the larger photocurrent of CdGDY and CdG (Fig. 3c and d) indicate lower charge transfer resistance and improved charge migration after combining the carbonaceous material with CdS, and the charge transfer ability of CdGDY is better than that of CdG.

The CO_2 adsorption performance of the different samples is traced in Fig. 4a, which shows that the introduction of graphdiyne or graphene promotes CO_2 adsorption on CdS. The maximum CO_2 adsorption capacity at $P/P_0 = 1.0$ for CdGDY, CdG and pure CdS is 0.12, 0.08, and 0.07 mmol g^{-1}, respectively. It is noted here that CdGDY shows a much higher CO_2 adsorption capacity than CdG, which is mainly attributed to the
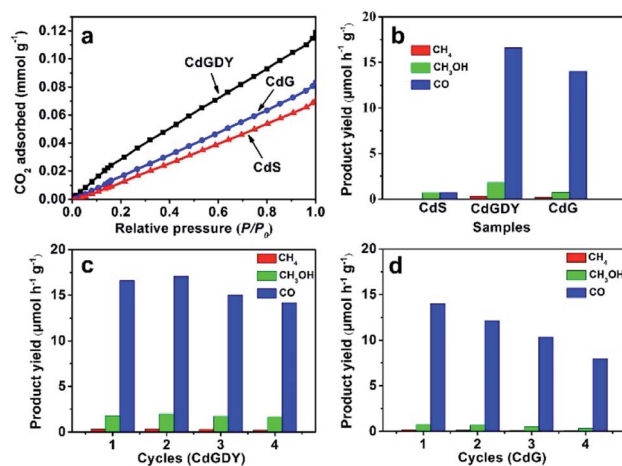

Fig. 4 CO_2 adsorption curves (a) of pure CdS, CdG and CdGDY; CH_4, CH_3OH and CO evolution during photocatalytic CO_2 reduction (b) over pure CdS, CdG and CdGDY; cycling tests of photocatalytic CO_2 reduction over CdGDY (c) and CdG (d).

hollow sites between the electron-deficient acetylenic linkages and sulfur vacancies serving as adsorption sites of CO_2 molecules. In addition, the relatively larger specific surface area of CdGDY than that of CdG can further increase the density of surface adsorption sites for CO_2 molecules.

The as-prepared photocatalysts were tested in photocatalytic gas-phase CO_2 reduction in the absence of a sacrificial agent. Control experiments were first performed and it was ascertained that there is no observable product in the absence of a photocatalyst, CO_2 or light irradiation. Table S3† lists the yields of the main products CO, CH_4, and CH_3OH, as well as the important by-product, H_2, over the different samples used in this study. It is found that the presence of carbon enhances the CO_2 photoreduction activity of CdS by more than one order of magnitude. It is interesting to note that better CO_2 photoreduction performance is achieved at a relatively low loading of graphdiyne or graphene; the maximum CO_2 conversion rate is as high as 18.72 and 14.97 μmol h^{-1} g^{-1} for CdGDY and CdG, respectively (see Fig. 4b and Table S3†), both of which are higher than or comparable to some typical results over graphene-based photocatalysts (Table S4†).The better activity of CdGDY than CdG is attributed to the more efficient interfacial charge transfer and higher CO_2 adsorption capacity, originating from the stronger interaction at the CdS/GDY interface as compared to the CdS/graphene interface, as well as the presence of more electron-deficient acetylenic linkages with hollow adsorption sites in graphdiyne. Moreover, only a small amount of H_2 was detected when using the different carbon-modified CdS. Importantly, the yield of H_2 is much lower than the conversion of CO_2, which demonstrates the high selectivity of CO_2 photoreduction on graphdiyne/graphene-supported CdS, as compared to hydrogen evolution. It is noteworthy that CdGDY exhibits relatively better selectivity than CdG (see Table S3†), which could also be attributed to the improved electronic properties resulting from the diacetylenic links.[36] Moreover, higher photocatalytic stability is found for CdGDY in

7674 | *J. Mater. Chem. A*, 2020, 8, 7671–7676

This journal is © The Royal Society of Chemistry 2020

comparison with CdG in a 4-cycle run of photocatalytic tests (see Fig. 4c and d). This is because the stronger interaction between CdS and graphdiyne ensures better structure stability of CdGdY. In addition, O_2 production is also detected (Fig. S10†), which is the product of water oxidation for the accomplishment of the photoredox cycle. To confirm that carbon in the reaction products originates solely from CO_2, gas chromatography-mass spectrometry (GC-MS) was employed to detect ^{12}CO and ^{13}CO when using isotope-labelled CO_2. As shown in Fig. S11,† when using $^{13}CO_2$ as the carbon source, the peak of ^{13}CO ($m/z = 29$) is significantly stronger than that of ^{12}CO ($m/z = 28$), and *vice versa*. These results prove that the carbon source for the photoreduction products is CO_2.

We have performed *in situ* FTIR during the photocatalytic process to further elucidate the reaction mechanism. When CdGDY is exposed to a mixture of CO_2 and water vapor, various species are generated (Fig. S12a†), including strongly adsorbed H_2O (1635 cm^{-1}), carbonate or bicarbonate (monodentate (m-CO_3^{2-}) at 1485 cm^{-1}, bidentate (b-CO_3^{2-}) at 1530 and 1306 cm^{-1}, and bicarbonate (HCO_3^-) at 1410 cm^{-1}), and CO_2^- species (1270 and 1660 cm^{-1}). Moreover, the IR intensity of CO_2^- species increases gradually with irradiation time (Fig. S12b†); signals due to primary HCO_3^- and CO_3^{2-} species are also enhanced. These results suggest that adsorbed CO_2 is transformed into CO_2^- on the surface of CdGDY due to the presence of numerous defect sites such as sulfur vacancies, which efficiently lower the reaction barrier, thereby ensuring strong adsorption and activation of CO_2 molecules.[55,56] Next, CO_2^- is converted into CO, CH_4, and CH_3OH along with by-products H_2 and O_2, *via* a series of reactions (Fig. S13†),[2,13,57] which describes a possible mechanism for CO_2 reduction.

In summary, using theoretical simulation and experimental characterization, we identify the chemical bonding between graphdiyne and CdS, which is stronger than the interfacial interaction between graphene and CdS. The resultant sulfur vacancies in CdS, together with the more electron-deficient acetylenic linkages in graphdiyne, give rise to sufficient CO_2 adsorption sites. Taking advantage of such strong interface coupling and improved CO_2 adsorption, more efficient electron transfer and storage can be achieved for the subsequent CO_2 reduction reaction. The obtained hybrid material of graphdiyne modified CdS thus shows more efficient photocatalytic reduction of wet CO_2 to chemical fuels in the gas phase without any sacrificial agent, with higher activity, stability and selectivity in comparison with the CdS/graphene photocatalyst. The unique properties of graphdiyne make it a rising star material for applications in solar energy conversion.

Conflicts of interest

There are no conflicts to declare.

Acknowledgements

References

1 D. Voiry, H. S. Shin, K. P. Loh and M. Chhowalla, *Nat. Rev. Chem.*, 2018, **2**, 0105.

2 M. Marszewski, S. W. Cao, J. G. Yu and M. Jaroniec, *Mater. Horiz.*, 2015, **2**, 261–278.

3 Y. Fang, Y. Ma, M. Zheng, P. Yang, A. M. Asiri and X. Wang, *Coord. Chem. Rev.*, 2018, **373**, 83.

4 J. R. Ran, M. Jaroniec and S. Z. Qiao, *Adv. Mater.*, 2018, **30**, 1704649.

5 C. Dong, M. Xing and J. Zhang, *Mater. Horiz.*, 2016, **3**, 608.

6 R. Shi, G. I. N. Waterhouse and T. R. Zhang, *Sol. RRL*, 2017, **1**, 1700126.

7 X. Li, J. Yu, M. Jaroniec and X. Chen, *Chem. Rev.*, 2019, **119**, 3962.

8 N. Zhang, M. Q. Yang, S. Q. Liu, Y. G. Sun and Y. J. Xu, *Chem. Rev.*, 2015, **115**, 10307.

9 J. Zhang, J. G. Yu, M. Jaroniec and J. R. Gong, *Nano Lett.*, 2012, **12**, 4584.

10 M. Q. Yang and Y. J. Xu, *Nanoscale Horiz.*, 2016, **1**, 185.

11 X. Li, J. G. Yu, S. Wageh, A. A. Al-Ghamdi and J. Xie, *Small*, 2016, **12**, 6640.

12 S. Chen, Y. Qi, C. Li, K. Domen and F. Zhang, *Joule*, 2018, **2**, 2260.

13 X. X. Chang, T. Wang and J. L. Gong, *Energy Environ. Sci.*, 2016, **9**, 2177.

14 M. M. Haley, S. C. Brand and J. J. Pak, *Angew. Chem., Int. Ed.*, 1997, **36**, 836.

15 G. Li, Y. Li, H. Liu, Y. Guo, Y. Li and D. Zhu, *Chem. Commun.*, 2010, **46**, 3256.

16 Y. S. Zhao, L. J. Zhang, J. Qi, Q. Jin, K. F. Lin and D. Wang, *Acta Phys.-Chim. Sin.*, 2018, **34**, 1048.

17 X. L. Lu, Y. Y. Han and T. B. Lu, *Acta Phys.-Chim. Sin.*, 2018, **34**, 1014.

18 Y. Zhao, H. Tang, N. Yang and D. Wang, *Adv. Sci.*, 2018, **5**, 1800959.

19 H. Yu, Y. Xue and Y. Li, *Adv. Mater.*, 2019, **31**, 1803101.

20 J. Li, J. Xu, Z. Xie, X. Gao, J. Zhou, Y. Xiong, C. Chen, J. Zhang and Z. Liu, *Adv. Mater.*, 2018, **30**, 1800548.

21 P. Y. Kuang, B. C. Zhu, Y. L. Li, H. B. Liu, J. G. Yu and K. Fan, *Nanoscale Horiz.*, 2018, **3**, 317.

22 Y. Zhao, J. Wan, H. Yao, L. Zhang, K. Lin, L. Wang, N. Yang, D. Liu, L. Song, J. Zhu, L. Gu, L. Liu, H. Zhao, Y. Li and D. Wang, *Nat. Chem.*, 2018, **10**, 924.

23 S. Wang, L. Yi, J. E. Halpert, X. Lai, Y. Liu, H. Cao, R. Yu, D. Wang and Y. Li, *Small*, 2012, **8**, 265.

24 N. L. Yang, Y. Y. Liu, H. Wen, Z. Y. Tang, H. J. Zhao, Y. L. Li and D. Wang, *ACS Nano*, 2013, **7**, 1504.

25 X. Zhang, M. Zhu, P. Chen, Y. Li, H. Liu, Y. Li and M. Liu, *Phys. Chem. Chem. Phys.*, 2015, **17**, 1217.

This journal is © The Royal Society of Chemistry 2020

J. Mater. Chem. A, 2020, **8**, 7671–7676 | **7675**

26 J. Li, Z. Xie, Y. Xiong, Z. Li, Q. Huang, S. Zhang, J. Zhou, R. Liu, X. Gao, C. Chen, L. Tong, J. Zhang and Z. Liu, *Adv. Mater.*, 2017, **29**, 1700421.

27 Y. Dong, Y. Zhao, Y. Chen, Y. Feng, M. Zhu, C. Ju, B. Zhang, H. Liu and J. Xu, *J. Mater. Sci.*, 2018, **53**, 8921.

28 S. Guo, Y. Jiang, F. Wu, P. Yu, H. Liu, Y. Li and L. Mao, *ACS Appl. Mater. Interfaces*, 2019, **11**, 2684–2691.

29 J. X. Lv, Z. M. Zhang, J. Wang, X. L. Lu, W. Zhang and T. B. Lu, *ACS Appl. Mater. Interfaces*, 2019, **11**, 2655–2661.

30 Y.-Y. Han, X.-L. Lu, S.-F. Tang, X.-P. Yin, Z.-W. Wei and T.-B. Lu, *Adv. Energy Mater.*, 2018, **8**, 1702992.

31 H.-Y. Si, C.-J. Mao, J.-Y. Zhou, X.-F. Rong, Q.-X. Deng, S.-L. Chen, J.-J. Zhao, X.-G. Sun, Y. M. Shen, W.-J. Feng, P. Gao and J. Zhang, *Carbon*, 2018, **132**, 598.

32 F. Xu, K. Meng, B. Zhu, H. Liu, J. Xu and J. Yu, *Adv. Funct. Mater.*, 2019, **29**, 1904256.

33 Z. Jia, Y. Li, Z. Zuo, H. Liu, C. Huang and Y. Li, *Acc. Chem. Res.*, 2017, **50**, 2470.

34 M. Q. Long, L. Tang, D. Wang, Y. L. Li and Z. G. Shuai, *ACS Nano*, 2011, **5**, 2593.

35 B. Wu, M. Li, S. Xiao, Y. Qu, X. Qiu, T. Liu, F. Tian, H. Li and S. Xiao, *Nanoscale*, 2017, **9**, 11939.

36 H. J. Kwon, Y. Kwon, T. Kim, Y. Jung, S. Lee, M. Cho and S. Kwon, *AIP Adv.*, 2017, **7**, 125013.

37 R. Liu, H. Liu, Y. Li, Y. Yi, X. Shang, S. Zhang, X. Yu, S. Zhang, H. Cao and G. Zhang, *Nanoscale*, 2014, **6**, 11336.

38 S. Y. Guo, H. L. Yan, F. Wu, L. J. Zhao, P. Yu, H. B. Liu, Y. L. Li and L. Q. Mao, *Anal. Chem.*, 2017, **89**, 13008.

39 L. L. Jiang, L. Y. Wang, G. S. Xu, L. N. Gu and Y. P. Yuan, *Sustainable Energy Fuels*, 2018, **2**, 430.

40 C. Hu, X. Zeng, J. Cui, H. Chen and J. Lu, *J. Phys. Chem. C*, 2013, **117**, 20998.

41 Y. Huang, Y. Liu, D. Zhu, Y. Xin and B. Zhang, *J. Mater. Chem. A*, 2016, **4**, 13626.

42 D. C. Jiang, Z. J. Sun, H. X. Jia, D. P. Lu and P. W. Du, *J. Mater. Chem. A*, 2016, **4**, 675.

43 X.-L. Yin, G.-Y. He, B. Sun, W.-J. Jiang, D.-J. Xue, A.-D. Xia, L.-J. Wan and J.-S. Hu, *Nano Energy*, 2016, **28**, 319.

44 J. F. Moulder, W. F. Stickle, P. E. Sobol and K. D. Bomben, *Handbook of X-Ray Photoelectron Spectroscopy*, Perkin-Elmer Corporation, Eden Prairie, MN, USA, 1992, p. 123.

45 D. J. Keeble, E. A. Thomsen, A. Stavrinadis, I. D. W. Samuel, J. M. Smith and A. A. R. Watt, *J. Phys. Chem. C*, 2009, **113**, 17306.

46 J. L. Davis, A. M. Chalifoux and S. L. Brock, *Langmuir*, 2017, **33**, 9434.

47 W. Zhou and H. Fu, *Inorg. Chem. Front.*, 2018, **5**, 1240.

48 Z. Fang, S. Weng, X. Ye, W. Feng, Z. Zheng, M. Lu, S. Lin, X. Fu and P. Liu, *ACS Appl. Mater. Interfaces*, 2015, **7**, 13915.

49 C. Gonzalez, B. Biel and Y. J. Dappe, *Phys. Chem. Chem. Phys.*, 2017, **19**, 9485.

50 H. Li, M. Huang and G. Cao, *Phys. Chem. Chem. Phys.*, 2016, **18**, 15110.

51 J. Lin, Y. Dong, Q. Zhang, D. Hu, N. Li, L. Wang, Y. Liu and T. Wu, *Angew. Chem., Int. Ed.*, 2015, **54**, 5103.

52 J. Xiong, Y. Liu, C. Cao, L. Shen, W. Wu, S. Liang, R. Liang and L. Wu, *J. Mater. Chem. A*, 2015, **3**, 6935.

53 B. Qiu, Q. Zhu, M. Du, L. Fan, M. Xing and J. Zhang, *Angew. Chem., Int. Ed.*, 2017, **56**, 2684.

54 B. Guo, L. Tian, W. Xie, A. Batool, G. Xie, Q. Xiang, S. U. Jan, R. Boddula and J. R. Gong, *Nano Lett.*, 2018, **18**, 5954.

55 H. Fujiwara, H. Hosokawa, K. Murakoshi, Y. Wada, S. Yanagida, T. Okada and H. Kobayashi, *J. Phys. Chem. B*, 1997, **101**, 8270.

56 M. Kanemoto, H. Hosokawa, Y. Wada, K. Murakoshi, S. Yanagida, T. Sakata, H. Mori, M. Ishikawa and H. Kobayashi, *J. Chem. Soc., Faraday Trans.*, 1996, **92**, 2401.

57 G. Yin, X. Huang, T. Chen, W. Zhao, Q. Bi, J. Xu, Y. Han and F. Huang, *ACS Catal.*, 2018, **8**, 1009.

7676 | *J. Mater. Chem. A*, 2020, **8**, 7671–7676

This journal is © The Royal Society of Chemistry 2020